Boost 2013 Report Title

Report of BOOST2013, hosted by the University of Arizona, 12th-16th of August 2013.

D. Adams[1], A. Arce[2], L. Asquith[3], M. Backovic[4], T. Barillari[5], P. Berta[6],
D. Bertolini[2], A. Buckley[8], J. Butterworth[9], R. C. Camacho Toro[10], J. Caudron[9],
Y.-T. Chien[11], J. Cogan[12], B. Cooper[9], D. Curtin[17], C. Debenedetti[18],
J. Dolen[9], M. Eklund[22], S. El Hedri[22], S. D. Ellis[22], T. Embry[22], D. Ferencek[23],
J. Ferrando[24], S. Fleischmann[16], M. Freytsis[25], M. Giulini[21], Z. Han[27],
D. Hare[4], P. Harris[4], A. Hinzmann[4], R. Hoing[4], A. Hornig[22], M. Jankowiak[4],
K. Johns[28], G. Kasieczka[23], T. Knight[24], G. Kasieczka[29], R. Kogler[30], W. Lampl[4],
A. J. Larkoski[4], C. Lee[31], R. Leone[31], P. Loch[31], D. Lopez Mateos[27], H. K. Lou[27],
M. Low[27], P. Maksimovic[32], I. Marchesini[32], S. Marzani[32], L. Masetti[33],
R. McCarthy[32], S. Menke[32], D. W. Miller[35], K. Mishra[36], B. Nachman[32], P. Nef[4],
F. T. O'Grady[24], A. Ovcharova[23], A. Picazio[37], C. Pollard[38], B. Potter Landua[29],
C. Potter[29], S. Rappoccio[39], J. Rutherfoord[40], G. P. Salam[10,11], J. Schabinger[23],
A. Schwartzman[4], M. D. Schwartz[27], B. Shuve[43], P. Sinervo[44], D. Soper[45],
D. E. Sosa Corral[45], M. Spannowsky[32], E. Strauss[34], M. Swiatlowski[4], J. Thaler[34],
C. Thomas[34], E. Thompson[1], N. V. Tran[36], J. Tseng[36], E. Usai[36], L. Valery[36],
J. Veatch[23], M. Vos[23], W. Waalewijn[4], and C. Young[47]

[1] *Columbia University, Nevis Laboratory, Irvington, NY 10533, USA*
[2] *Duke University, Durham, NC 27708, USA*
[3] *Argonne National Laboratory, Lemont, IL 60439, USA*
[4] *SLAC National Accelerator Laboratory, Menlo Park, CA 94025, USA*
[5] *Deutsches Elektronen-Synchrotron, DESY, D-15738 Zeuthen, Germany*
[6] *Cornell University, Ithaca, NY 14853, USA*
[7] *Lund University, Lund, SE 22100, Sweden*
[8] *University of Edinburgh, EH9 3JZ, UK*
[9] *University College London, WC1E 6BT, UK*
[10] *LPTHE, UPMC Univ. Paris 6 and CNRS UMR 7589, Paris, France*
[11] *CERN, CH-1211 Geneva 23, Switzerland*
[12] *CAFPE and U. of Granada, Granada, E-18071, Spain*
[13] *McGill University, Montreal, Quebec H3A 2T8, Canada*
[14] *Iowa State University, Ames, Iowa 50011, USA*
[15] *Rutgers University, Piscataway, NJ 08854, USA*
[16] *Bergische Universitaet Wuppertal, Wuppertal, D-42097, Germany*
[17] *YITP, Stony Brook University, Stony Brook, NY 11794-3840, USA*
[18] *University of Manchester, Manchester, M13 9PL, UK*
[19] *UNESP - Universidade Estadual Paulista, Sao Paulo, 01140-070, Brazil*
[20] *INFN and University of Naples, IT80216, Italy*
[21] *University of Geneva, CH-1211 Geneva 4, Switzerland*
[22] *University of Washington, Seattle, WA 98195, USA*
[23] *Instituto de Física Corpuscular, IFIC/CSIC-UVEG, E-46071 Valencia, Spain*
[24] *University of Glasgow, Glasgow, G12 8QQ, UK*
[25] *Berkeley National Laboratory, University of California, Berkeley, CA 94720, USA*
[26] *Universidad de Buenos Aires, AR-1428, Argentina*
[27] *Harvard University, Cambridge, MA 02138, USA*
[28] *Weizmann Institute, 76100 Rehovot, Israel*
[29] *Universitaet Hamburg, DE-22761, Germany*
[30] *Universitaet Heidelberg, DE-69117, Germany*
[31] *University of Arizona, Tucson, AZ 85719, USA*
[32] *IPPP, University of Durham, Durham, DH1 3LE, UK*
[33] *Universitaet Mainz, DE 55099, Germany*
[34] *MIT, Cambridge, MA 02139, USA*
[35] *University of Chicago, IL 60637, USA*
[36] *Fermi National Accelerator Laboratory, Batavia, IL 60510, USA*
[37] *Indiana University, Bloomington, IN 47405, USA*
[38] *University of California, Davis, CA 95616, USA*
[39] *Johns Hopkins University, Baltimore, MD 21218, USA*
[40] *INFN and University of Pisa, Pisa, IT-56127, Italy*
[41] *Texas A & M University, College Station, TX 77843, USA*
[42] *INFN and University of Calabria, Rende, IT-87036, Italy*
[43] *Brown University, Richmond, RI 02912, USA*
[44] *Yale University, New Haven, CT 06511, USA*
[45] *CEA Saclay, Gif-sur-Yvette, FR-91191, France*
[46] *University of Illinois, Chicago, IL 60607, USA*
[47] *University of California, Berkeley, CA 94720, USA*

Abstract Abstract for BOOST2013 report

1 Introduction

Jet substructure has been around a while now, and it's
time to study the correlations between the plethora of
observables that have been developed and used. Previ-
ous BOOST reports [1,2,3] studied some of these things.

2 Monte Carlo Samples

Give details about how the samples we use have been
generated.

3 Jet Algorithms and Grooming Approaches

Describe the jet algorithms and grooming approaches
that we will use in the report. Give the nomenclature
that we will use to refer to e.g. the groomed mass in
the rest of the report.

4 Substructure Variables/Taggers

Describe the specific substructure variables and tag-
ging approaches that we will be using in this report
e.g. n-subjettiness, Q-jets, HTT, JH tagger. Give the
nomenclature that we will use to refer to these vari-
ables/taggers in the rest of the report.

5 Quark-Gluon Discrimination

In this section we examine the differences between quark
and gluon initiated jets in terms of the substructure
variables, and to what extent these variables are corre-
lated. Along the way, we attempt to provide some the-
oretical understanding of these observations. The moti-
vation for these studies comes not only from the desire
to "tag" a jet as being quark or gluon initiated, but also
from the point of view of understanding the quark and
gluon components to the QCD background to boosted
boson and boosted top tagging.

5.1 Methodology

These studies use the XXX samples described previ-
ously in Section 2.

Jets are reconstructed using the XXX jet algorithms
described in Section 3. The following event selection is
then applied to these samples....(presumably this will
vary depending on which kinematic bin is used, as will
the actual samples used - maybe summarize in a table).

Figure 1 shows background versus signal in some
basic kinematic distributions. *Do we want to reweight
quark kinematics to gluon or vice versa?*

5.2 Single Variable Discrimination

Figure 2 the compares the quark and gluon samples in
the mass distributions for the different groomers, and
Figure 3 in the different substructure variables.

Figure 4 shows the single variable ROC curves in
the p_T 500 GeV bin for the anti-k_T R=0.8 algorithm,
compared to the ROC curve for a BDT combination of
all the variables. Only the ungroomed mass is shown.
One can see that the single most discriminant variables
are n_constits and $C_1^{\beta=0}$.

We want to look also at:

- *Dependence on R.*
- *Dependence on pT.*

5.3 Correlations

*Put in 2-D plots of correlations between variables (see
theory discussions below)*

5.4 Combined Performance of Quark-Gluon Tagging

Put in ROC curves of BDT combination of variables

5.5 QJets Volatility and $p_T D$ ($C_1^{(\beta=0)}$)

Simple explanation of correlation, or why does com-
bining volatility and $p_T D$ improve quark versus gluon
discrimination. $p_T D$ ($C_1^{(\beta=0)}$) takes small (large) values
for a jet with near-democratic energy sharing between
particles and large (small) values when the energy of
the jet is contained in a few particles. Because we ex-
pect gluons to radiate more particles, we expect that
$p_T D_g < p_T D_q$ (or $C_1^{(\beta=0)}{}_g > C_1^{(\beta=0)}{}_q$). Now, we expect
the volatility of gluon jets to be in general smaller than
that of quark jets because there is a greater probability
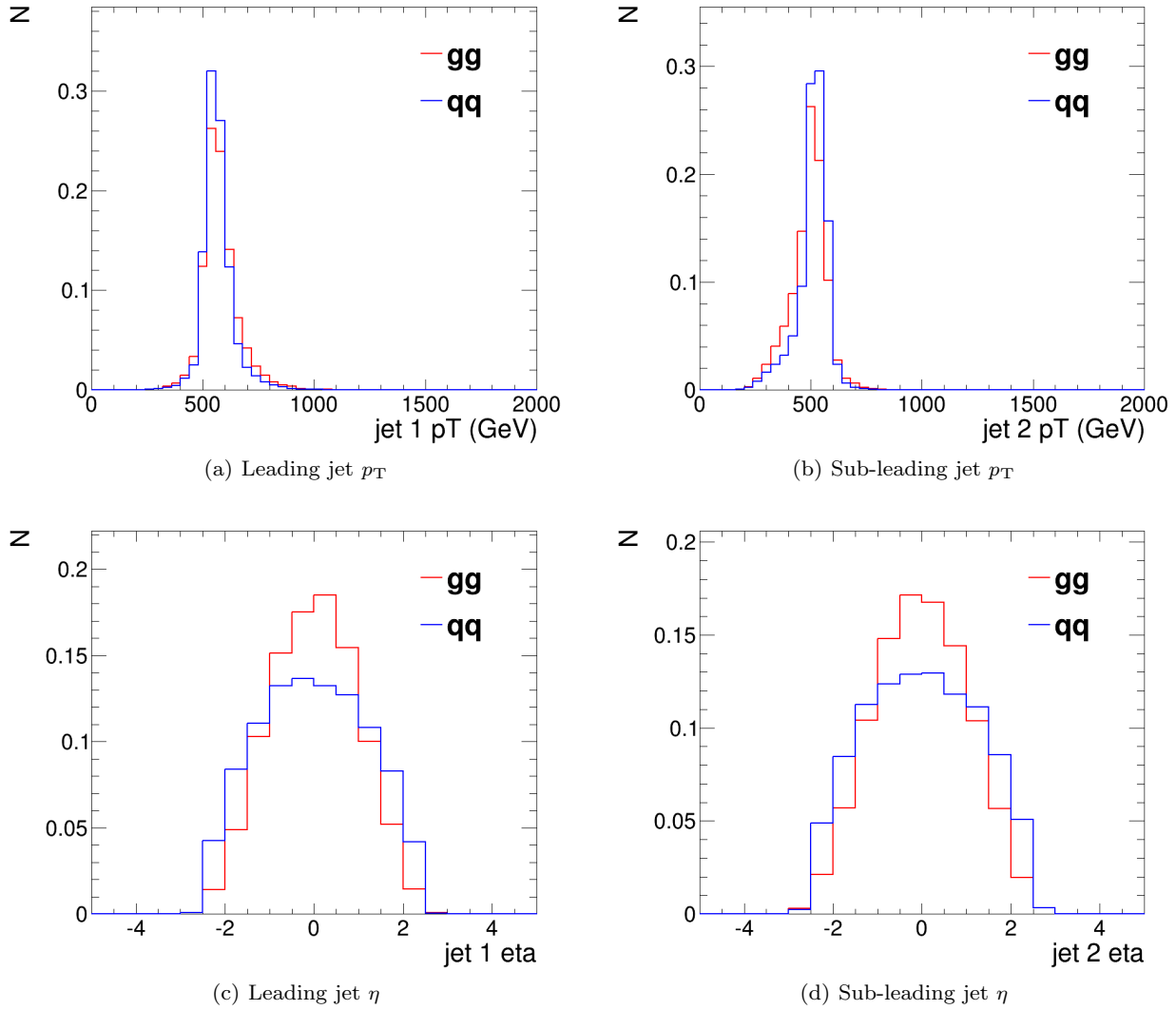(by a factor of about $C_A/C_F = 9/4$) that there was a

(a) Leading jet p_T

(b) Sub-leading jet p_T

(c) Leading jet η

(d) Sub-leading jet η

Fig. 1 Comparisons of quark and gluon distributions in the p_T 500 GeV bin using the anti-k_T R=0.8 algorithm: basic kinematic distributons.

relatively hard emission in a jet that is not groomed away. By measuring both volatility and $p_T D$, we are sensitive to both regions of phase space: where a relatively hard emission dominates the mass of the jet as well as the region where many soft emissions set the jet mass.

The following is Steve's discussion of volatility difference between quarks and gluons:

Here is the (qualitative) thinking: typical QCD jet mass distributions look as illustrated on slide 17, although you should really be thinking in terms of plot versus m/p_T, since p_T is what sets the scale in the plot. Qualitatively there is a (very) large peak for $m/p_T \lesssim 0.1$ and you should think of these jets as having masses that arise from multiple soft emissions, some of which are at substantial angles. It is these components of the

jet that are operated on by pruning (reducing the mass dramatically) and that yield the large volatility tail for QCD jets. For larger m/p_T values there is typically a shoulder (my description is clearest on a semi-log plot) that runs out to about $m/pT \sim 0.40.5$ (where the distribution decreases rapidly). These are the QCD jets (a small fraction of the total in a given p_T bin) that contain a hard, relatively large angle emission, which supplies the bulk of the jet mass. Such jets are effected only slightly by pruning and should exhibit much smaller volatility than the jets in the (smaller mass) peak region.

With that picture in mind and recalling that the size of the shoulder is given by low order perturbation theory (the probability of the one hard emission), we expect that the shoulder will be higher for gluons than
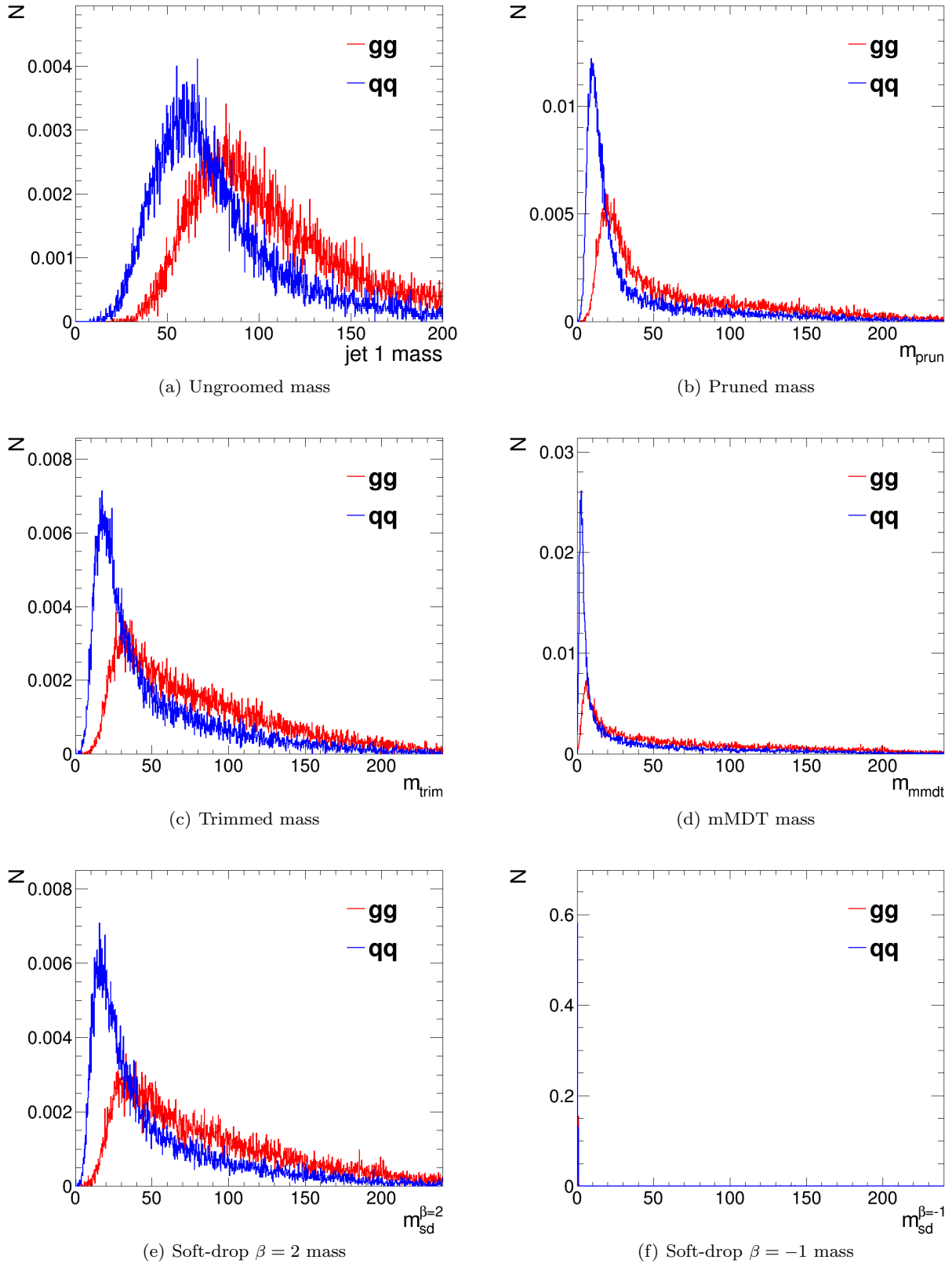
(a) Ungroomed mass

(b) Pruned mass

(c) Trimmed mass

(d) mMDT mass

(e) Soft-drop $\beta = 2$ mass

(f) Soft-drop $\beta = -1$ mass

Fig. 2 Comparisons of quark and gluon distributions in the p_T 500 GeV bin using the anti-k_T R=0.8 algorithm: leading jet mass distributions.
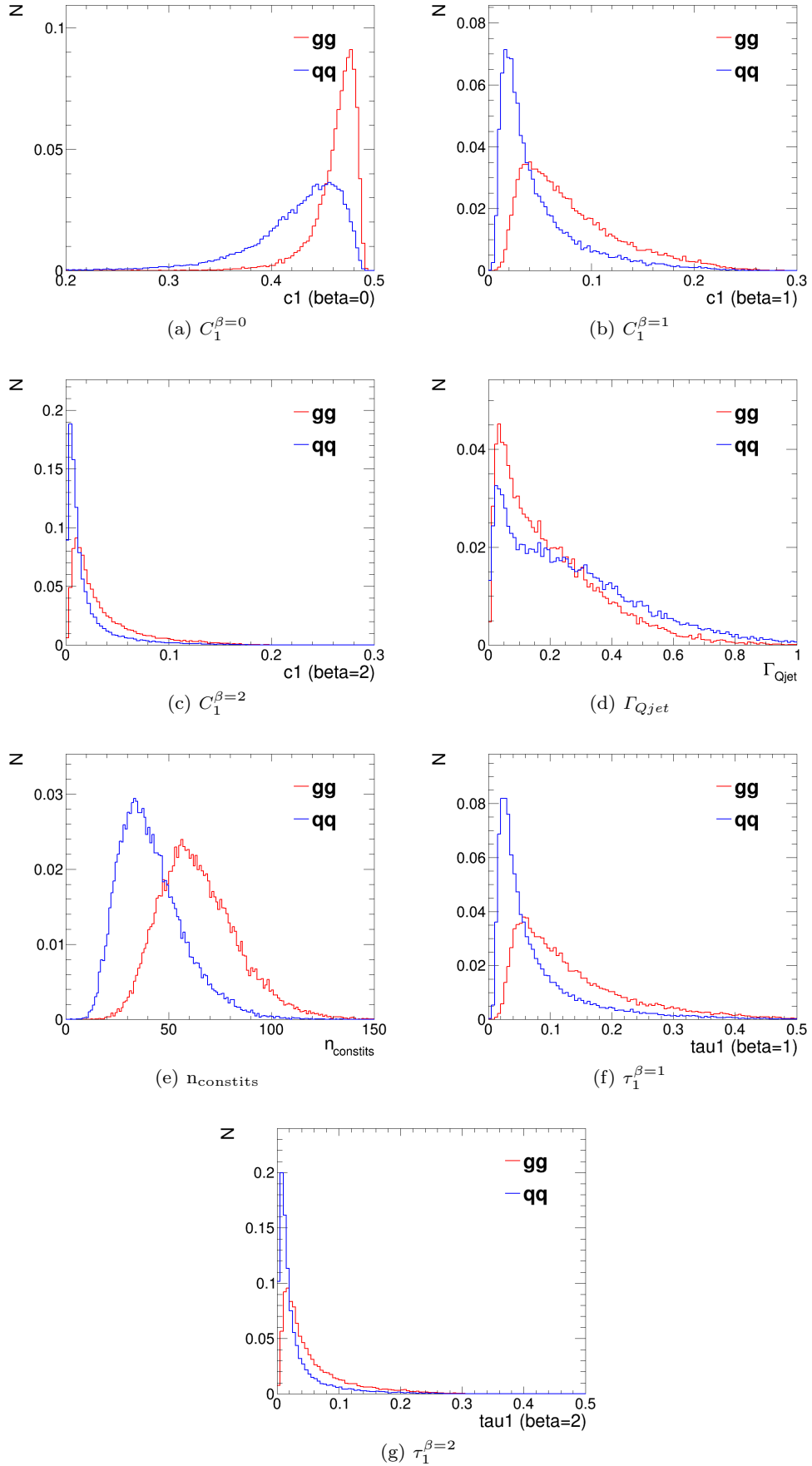
(a) $C_1^{\beta=0}$

(b) $C_1^{\beta=1}$

(c) $C_1^{\beta=2}$

(d) Γ_{Qjet}

(e) $n_{constits}$

(f) $\tau_1^{\beta=1}$

(g) $\tau_1^{\beta=2}$

Fig. 3 Comparisons of the QCD background to the WW signal in the p_T 500 GeV bin using the anti-k_T R=0.8 algorithm: substructure variables.
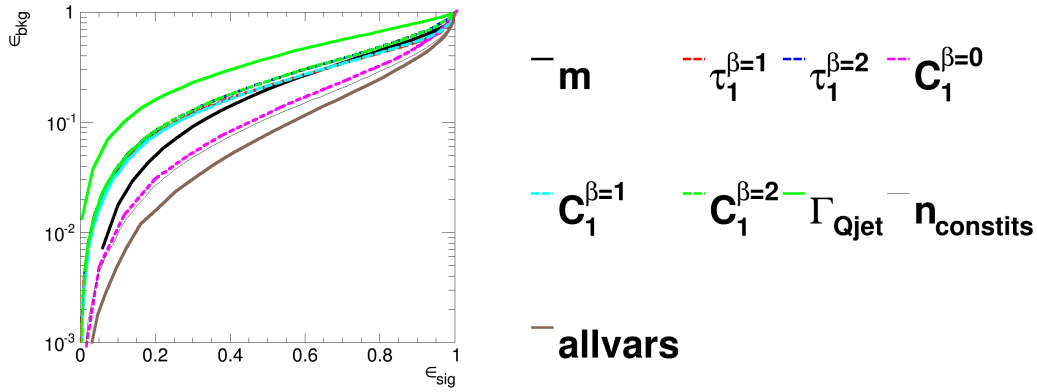
Fig. 4 The ROC curve for all single variables considered for quark-gluon discrimination in the p_T 500 GeV bin using the anti-k_T R=0.8 algorithm.

for quarks (essentially by the usual C_A/C_F color charge factor), as suggested by the lower right plot on slide 17. Since the shoulder presumably plays a more important role for gluons (since it is larger), one would expect that the volatility distribution for gluons is narrower than quarks, as suggested in the upper left plot on slide 17. Am I making sense?

On the other hand, the volatility distribution plot indicates that the Q vs G distributions for your cuts are not really very different, which is presumably why it is not a very good discriminant by itself. But I expect this to depend it detail on where we are operating on the m/pT distributions. This leads to my request above. Your p_T bin is pretty broad and I dont expect the q and g samples to have the same shape within the bin. Of course, this may not be an issue, but I would like to check.

5.6 Comparison of Groomed Jet Masses

6 Boosted W-Tagging

In this section we study the performance of various jet algorithms in combination with jet substructure variables/taggers in terms of the identification of a boosted hadronically decaying W signal. For each jet algorithm we produce Receiver Operating Characteristic (ROC) curves that elucidate the performance of various variables that are capable of providing discrimination between a hadronic W signal and a QCD jet. These variables are then combined in a Boosted Decision Tree (BDT) and the performance of the resulting BDT discriminant explored through ROC curves to understand the degree to which variables are correlated and exploiting the same information. These studies are repeated in different kinematic regimes, to explore both the perfor-

mance and correlations as a function of the jet boost, and where substructure approaches may break down.

6.1 Methodology

These studies use the $X \rightarrow WW$ samples as signal and the XXX samples to model the QCD background.

Jets are reconstructed using the XXX jet algorithms described in the previous section. The following event selection is then applied to these samples....(presumably this will vary depending on which kinematic bin is used, as will the actual samples used - maybe summarize in a table).

Figure 5 shows background versus signal in some basic kinematic distributions. *Do we want to reweight signal kinematics to background or vice versa? Do we want to study quarks/gluons separately?*

Go on to explain how we produce the ROC curves.

6.2 Performance at Moderate Boosts

(this section is to cover the W-tagging performance for jet p_T 200-300 GeV and 500-600 GeV using $\sqrt{s} = 8$ TeV samples)

6.2.1 Single Variable Performance

Show plots of signal versus background for all single variables investigated.

Figure 6 the compares signal and background in the mass distributions for the different groomers, and Figure 7 in the different substructure variables.

Figure 8 shows the single variable ROC curves in the p_T 500 GeV bin for the anti-k_T R=0.8 algorithm, compared to the ROC curve for a BDT combination of
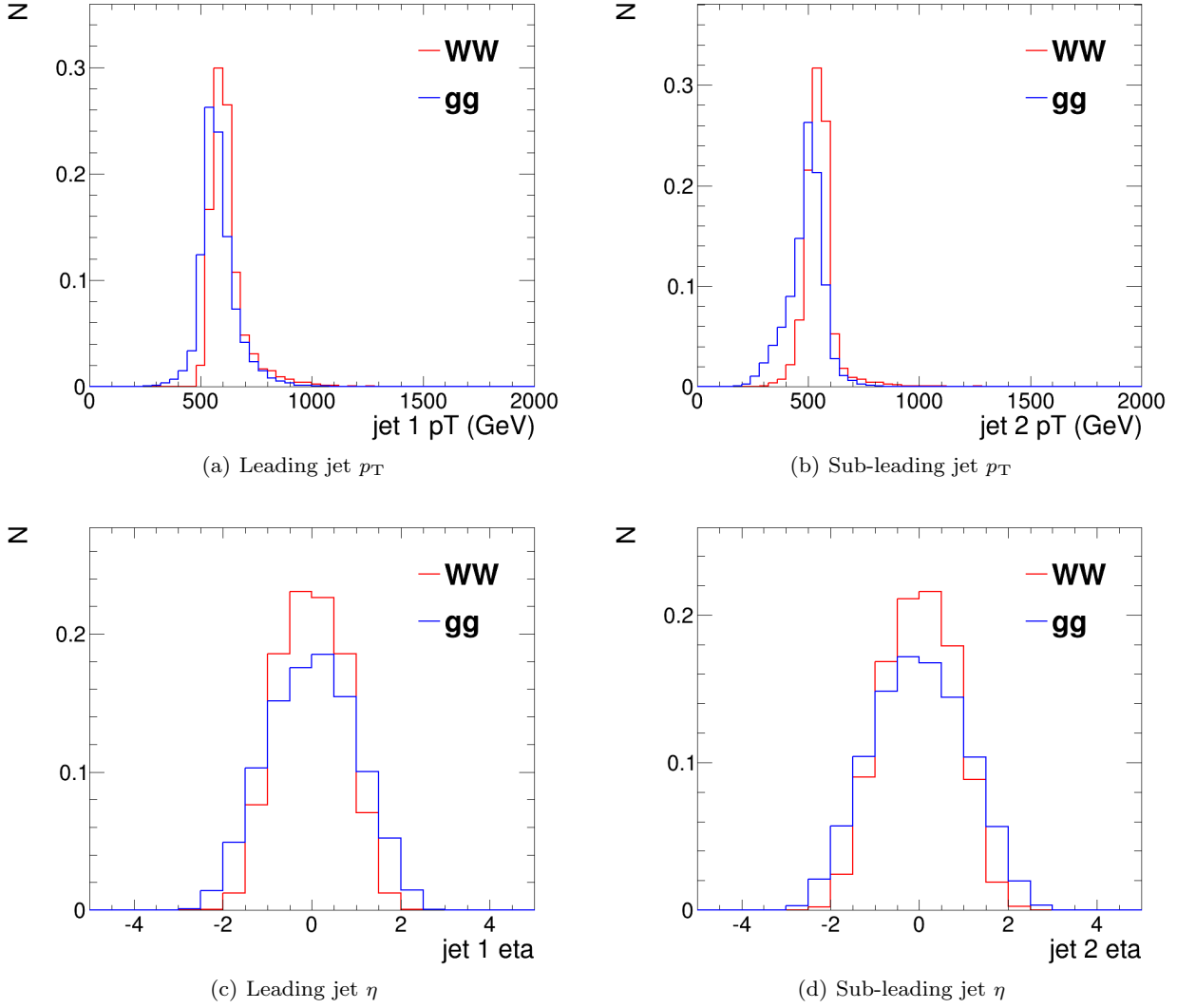
(a) Leading jet p_T

(b) Sub-leading jet p_T

(c) Leading jet η

(d) Sub-leading jet η

Fig. 5 Comparisons of the QCD background to the WW signal in the p_T 500 GeV bin using the anti-k_T R=0.8 algorithm: basic kinematic distributons.

all the variables. One can see that the best performant single variables for a reasonable signal efficiency are the groomed/filtered masses, which all have a similar level of performance with the exception of the soft drop mass with $\beta = -1$. *Would be good to split this into two plots, one using the masses and one for other variables, or somehow make the mass and other variable curves more distinct from one another by using same colour for all the mass curves.*

We want to look also at:

- *Dependence on R. So have the same single variable ROC for e.g. R=1.2, R=0.4. Then possibly have another plot which compares the best single variable (e.g. groomed mass) for different R.*
- *Dependence on pT. Again want to repeat the plot for different kinematic bins, and then have a plot which*

compares the best performance in each kinematic bin to see the dependence of performance on kinematics.

Figure 9 shows the single variable ROC curves in the p_T 500 GeV bin for the anti-k_T R=1.2 algorithm, compared to the ROC curve for a BDT combination of all the variables. Comparing to Figure 8, one can see that the performance of the groomed masses is quite similar. However, the performance of the other non-mass substructure variables is markedly different, and better in the R=0.8 case.
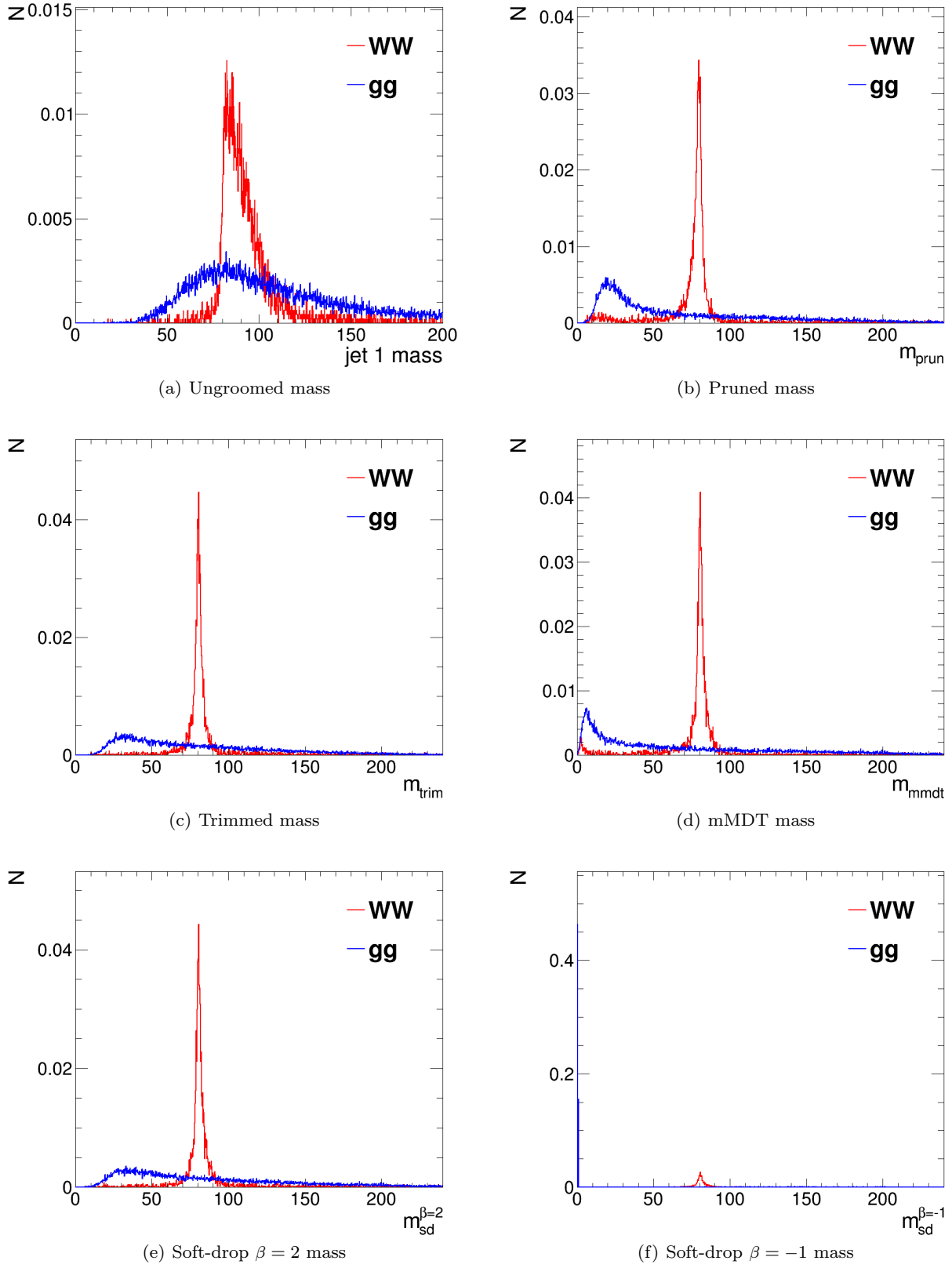
(a) Ungroomed mass

(b) Pruned mass

(c) Trimmed mass

(d) mMDT mass

(e) Soft-drop $\beta = 2$ mass

(f) Soft-drop $\beta = -1$ mass

Fig. 6 Comparisons of the QCD background to the WW signal in the p_T 500 GeV bin using the anti-k_T R=0.8 algorithm: leading jet mass distributions.
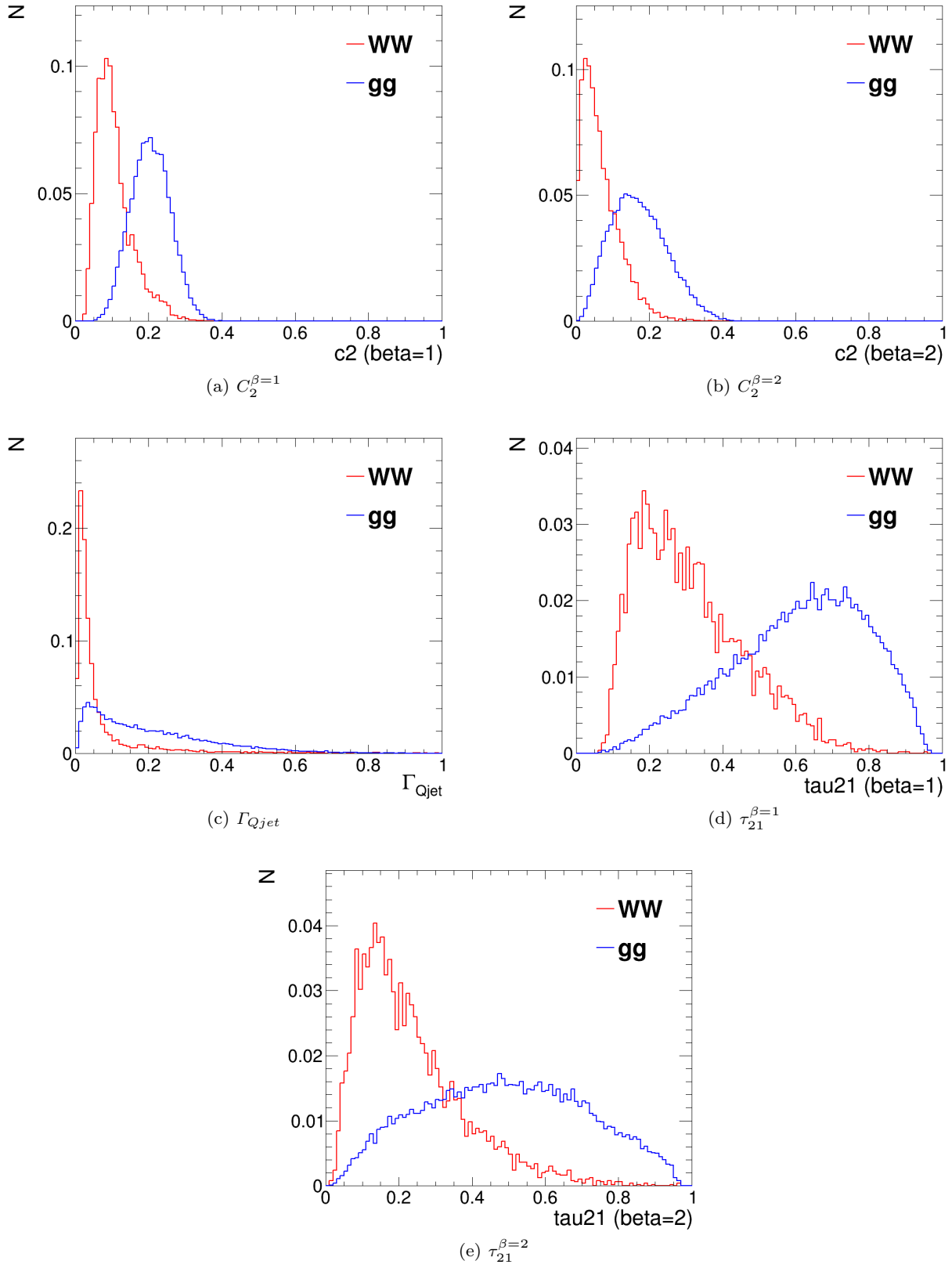
(a) $C_2^{\beta=1}$

(b) $C_2^{\beta=2}$

(c) Γ_{Qjet}

(d) $\tau_{21}^{\beta=1}$

(e) $\tau_{21}^{\beta=2}$

Fig. 7 Comparisons of the QCD background to the WW signal in the p_T 500 GeV bin using the anti-k_T R=0.8 algorithm: substructure variables.
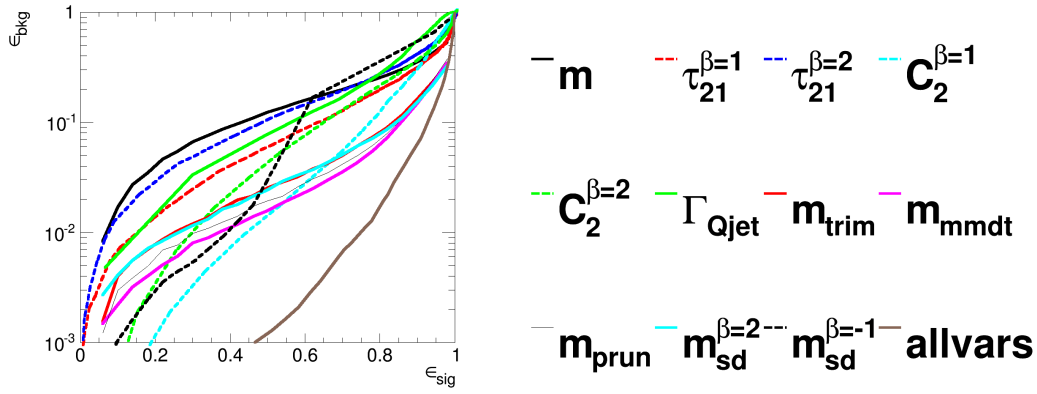
Fig. 8 The ROC curve for all single variables considered for W tagging in the p_T 500 GeV bin using the anti-k_T R=0.8 algorithm.
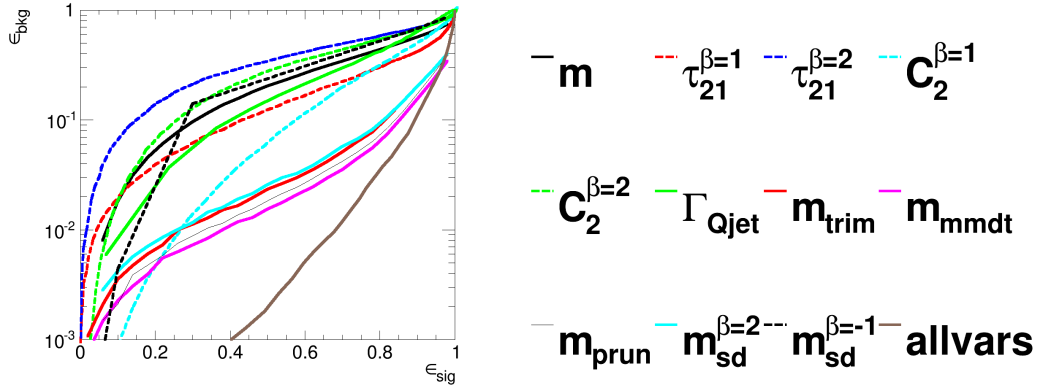

Fig. 9 The ROC curve for all single variables considered for W tagging in the p_T 500 GeV bin using the anti-k_T R=1.2 algorithm.

6.2.2 Combined Performance

Mass + X Performance

Figure 10 shows the BDT combinations of each mass variable with every other variable considered in the p_T 500 GeV bin using the anti-k_T R=0.8 algorithm. *Can we drop the combinations of mass + mass from these plots to make them clearer? Also would be good to put the single variable mass curve on these plots, so you can see how much improvement the combination gives, and the "all variables" curve.*

No combination with other variables can recover the poor performance of the ungroomed mass and the soft drop mass with $\beta = -1$. The other groomed/filtered masses are all most improved by combination with the $C_2^{\beta=1}$ energy correlation function. Figure 11 shows the 2-D correlation plots between the mMDT mass and the $C_2^{\beta=1}$, Γ_{Qjet} and $\tau_{21}^{\beta=1}$ variables. One can clearly see that there is substantially less correlation between the

mass and $C_2^{\beta=1}$ than the other variables. Similar results are seen for the other groomed masses.

Figure 13 shows the BDT combinations of the bset performant groomed masses with every other variable considered in the p_T 500 GeV bin using the anti-k_T R=1.2 algorithm. Interestingly, the groomed masses are now all most improved by combination with the $\tau_{21}^{\beta=1}$ variable, in contrast with $C_2^{\beta=1}$ which performed best for the smaller radius of R=0.8. One can see from Figure 9 that the single variable discrimination of $\tau_{21}^{\beta=1}$ and $C_2^{\beta=1}$ changes quite markedly when the distance parameter R is varied, although in both cases $C_2^{\beta=1}$ is a better single variable discriminant (except for very high signal efficiencies). Figure 12 shows how the actual distributions of the $C_2^{\beta=1}$ and $\tau_{21}^{\beta=1}$ change when we change the distance parameter. Figure 14 shows the 2-D correlation plots between between the mMDT mass and the $C_2^{\beta=1}$, Γ_{Qjet} and $\tau_{21}^{\beta=1}$ variables for the R=1.2 case. It is hard to see a substantial difference in the correlations here versus Figure 11, but perhaps $C_2^{\beta=1}$
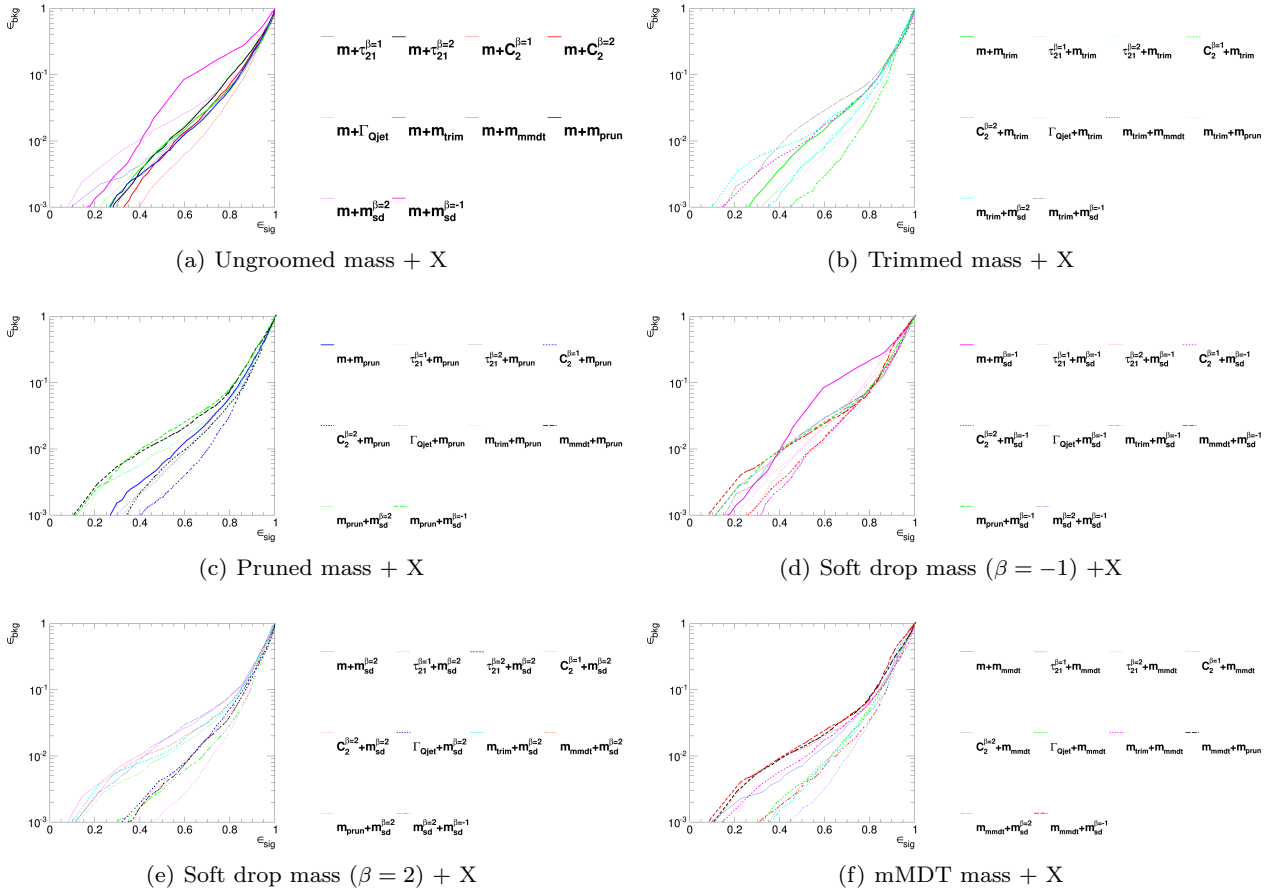
(a) Ungroomed mass + X

(b) Trimmed mass + X

(c) Pruned mass + X

(d) Soft drop mass ($\beta = -1$) +X

(e) Soft drop mass ($\beta = 2$) + X

(f) mMDT mass + X

Fig. 10 The BDT combinations of each mass variable with every other variable considered in the p_T 500 GeV bin using the anti-k_T R=0.8 algorithm.

is marginally more correlated with the mass for R=1.2 compared to R=0.8.

Now show a plot which compares on one plot the best combined performance for each groomed mass + X for both R=0.8 and 1.2 cases e.g. mass + $C_2^{\beta=1}$ for R=0.8 and mass + $\tau_{21}^{\beta=1}$ for R=1.2, and draw on also the all variables curve for both R=0.8,1.2. Then we can see if there is much dependence on choice of mass once you combine with another variable, and compare directly the two distance parameters. This plot is just for one kinematic bin, we should make the same plot for others.

Repeat these studies for different R and different kinematic bins. Finally make plots which compare best combined performance for different R and kinematics.

Do we want to look at other combinations of variables which don't involve mass? Practically I think we will always be making mass + X though.

Mass + Mass Performance

It's interesting also to study and understand how the different groomed masses relate to each other and how they are correlated.

Figures 15 and Figures 16 shows 2-D correlation plots of the different types of groomed mass in the p_T 500 GeV bin using the anti-k_T R=0.8 algorithm.

Worth also showing some ROC curves for mass + mass combinations?

6.3 Performance at High Boosts

(this section is to cover the W-tagging performance for jet p_T 1-1.1 TeV and > 1.5 TeV using $\sqrt{s} = 14$ TeV samples)

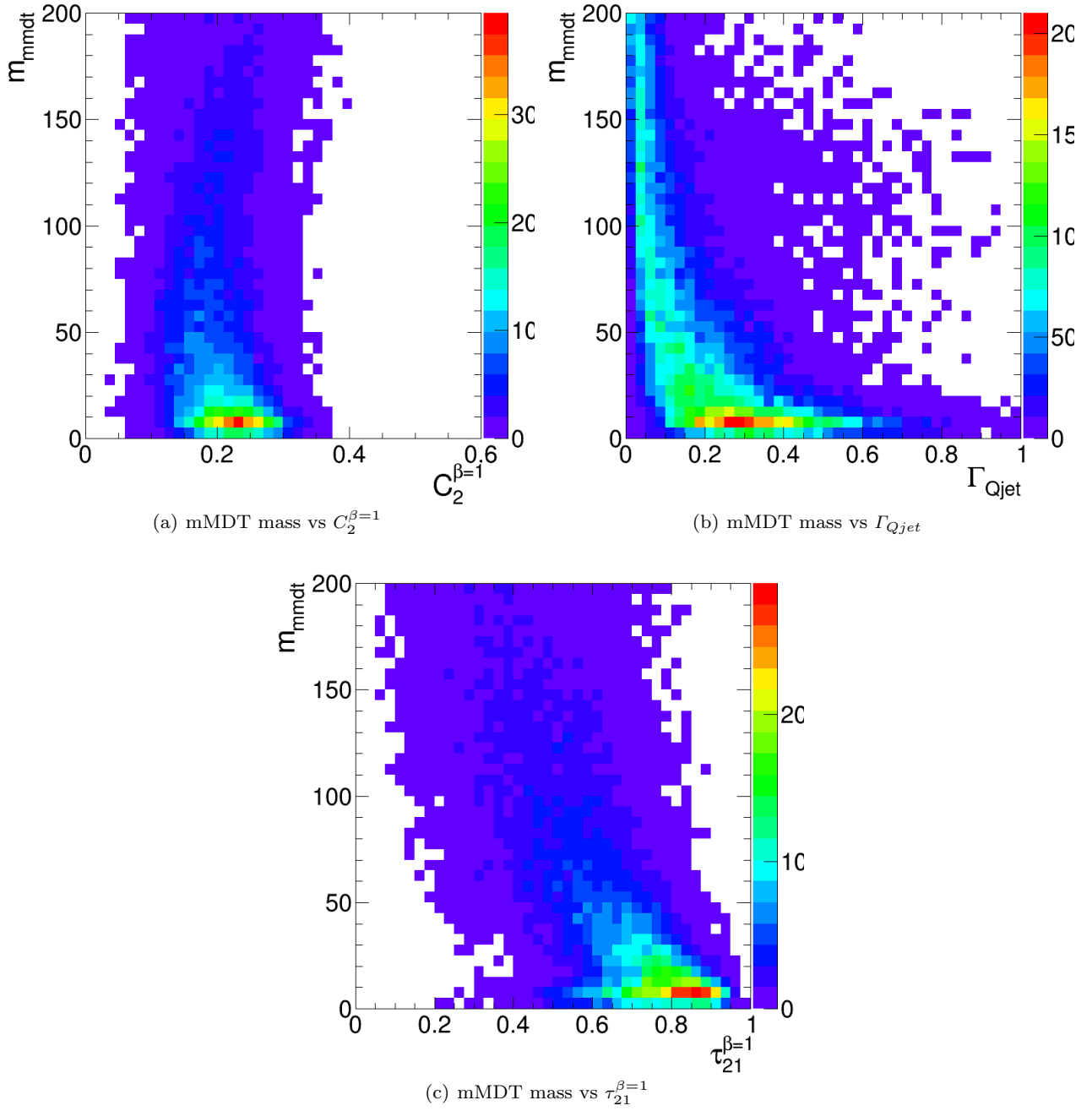*Maybe we don't need to divide into different medium/high boost sections.*

(a) mMDT mass vs $C_2^{\beta=1}$

(b) mMDT mass vs Γ_{Qjet}

(c) mMDT mass vs $\tau_{21}^{\beta=1}$

Fig. 11 2-D plots showing the correlation between mMDT mass and various substructure variables in the p_T 500 GeV bin using the anti-k_T R=0.8 algorithm in the gg sample.

(a) $C_2^{\beta=1}$, R=0.8

(b) $C_2^{\beta=1}$, R=1.2

(c) $\tau_{21}^{\beta=1}$, R=0.8
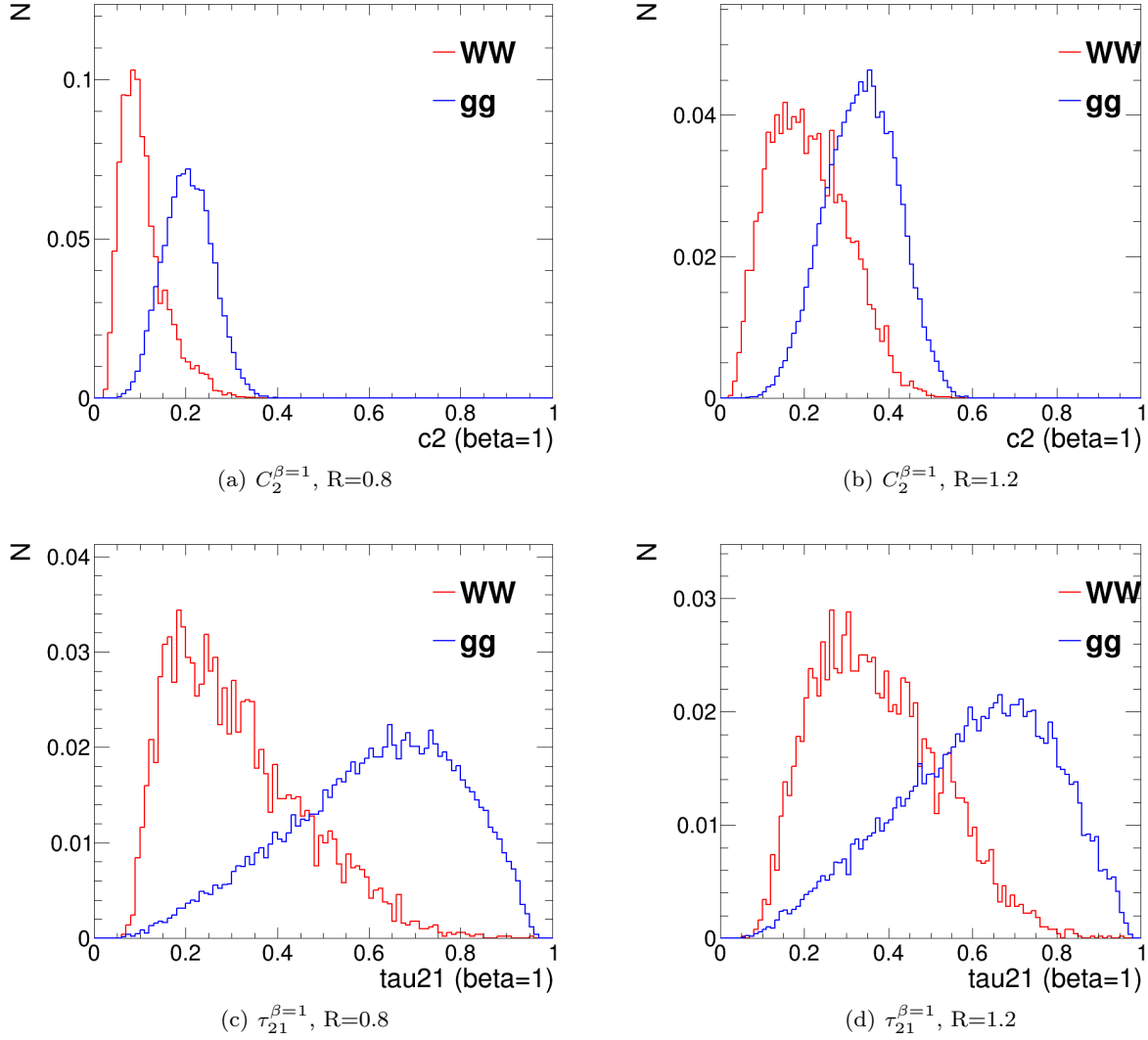
(d) $\tau_{21}^{\beta=1}$, R=1.2

Fig. 12 Comparisons of the QCD background to the WW signal in the p_T 500 GeV bin for $C_2^{\beta=1}$ and $\tau_{21}^{\beta=1}$ variables and using the R=0.8 and R=1.2 anti-k_T distance parameters.

Table 1 Action of various groomers on the jet mass distribution in the different phase space regions. For pruning, $a_{\mathrm{prune}} = z_{\mathrm{cut}}R_0$ and for trimming $a_{\mathrm{trim}} = \sqrt{z_{\mathrm{cut}}}R_{\mathrm{sub}}$.

Action	Pruning	Trimming	mMDT	SD ($\beta > 0$)
$m > \sqrt{z_{\mathrm{cut}}}R_0 p_T$	–	–	–	–
$m < \sqrt{z_{\mathrm{cut}}}R_0 p_T$ $m > a_x p_T$	cuts soft & soft-collinear	cuts soft & soft-collinear	cuts soft & soft-collinear	cuts soft & partially (β) on soft-collinear
$m < a_x p_T$	cuts partially on both soft & soft-collinear	–	cuts soft & soft-collinear	cuts soft & partially (β) on soft-collinear

(a) Trimmed mass + X

(b) Pruned mass + X

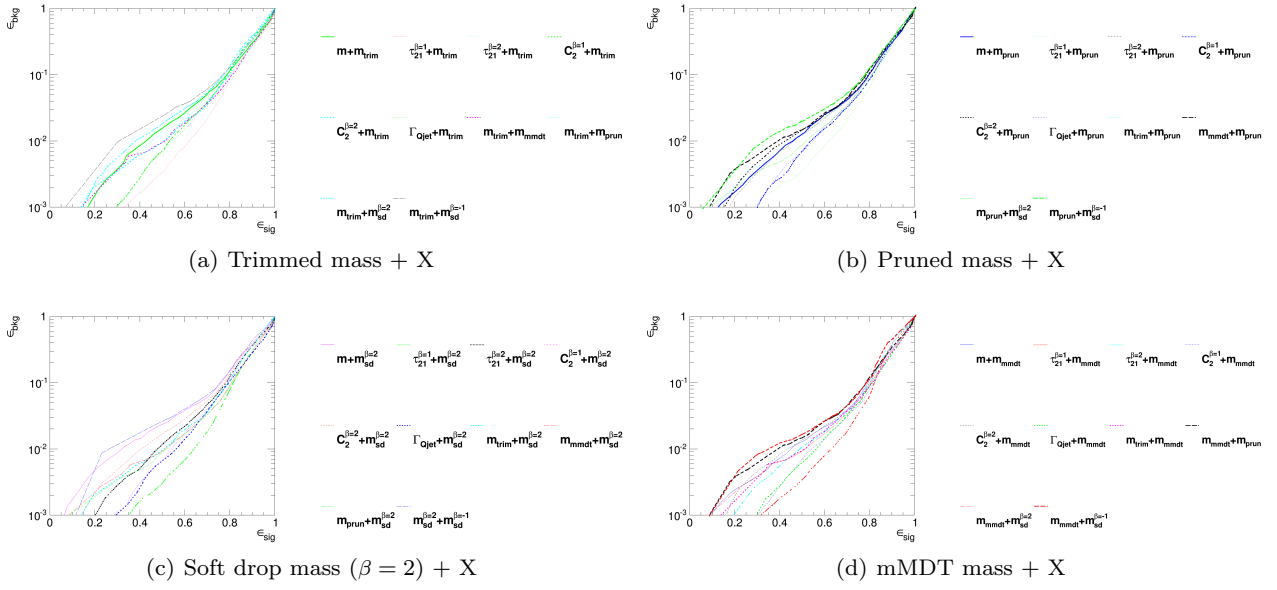(c) Soft drop mass ($\beta = 2$) + X

(d) mMDT mass + X

Fig. 13 The BDT combinations of each mass variable with every other variable considered in the p_T 500 GeV bin using the anti-k_T R=1.2 algorithm.

(a) mMDT mass vs $C_2^{\beta=1}$

(b) mMDT mass vs Γ_{Qjet}

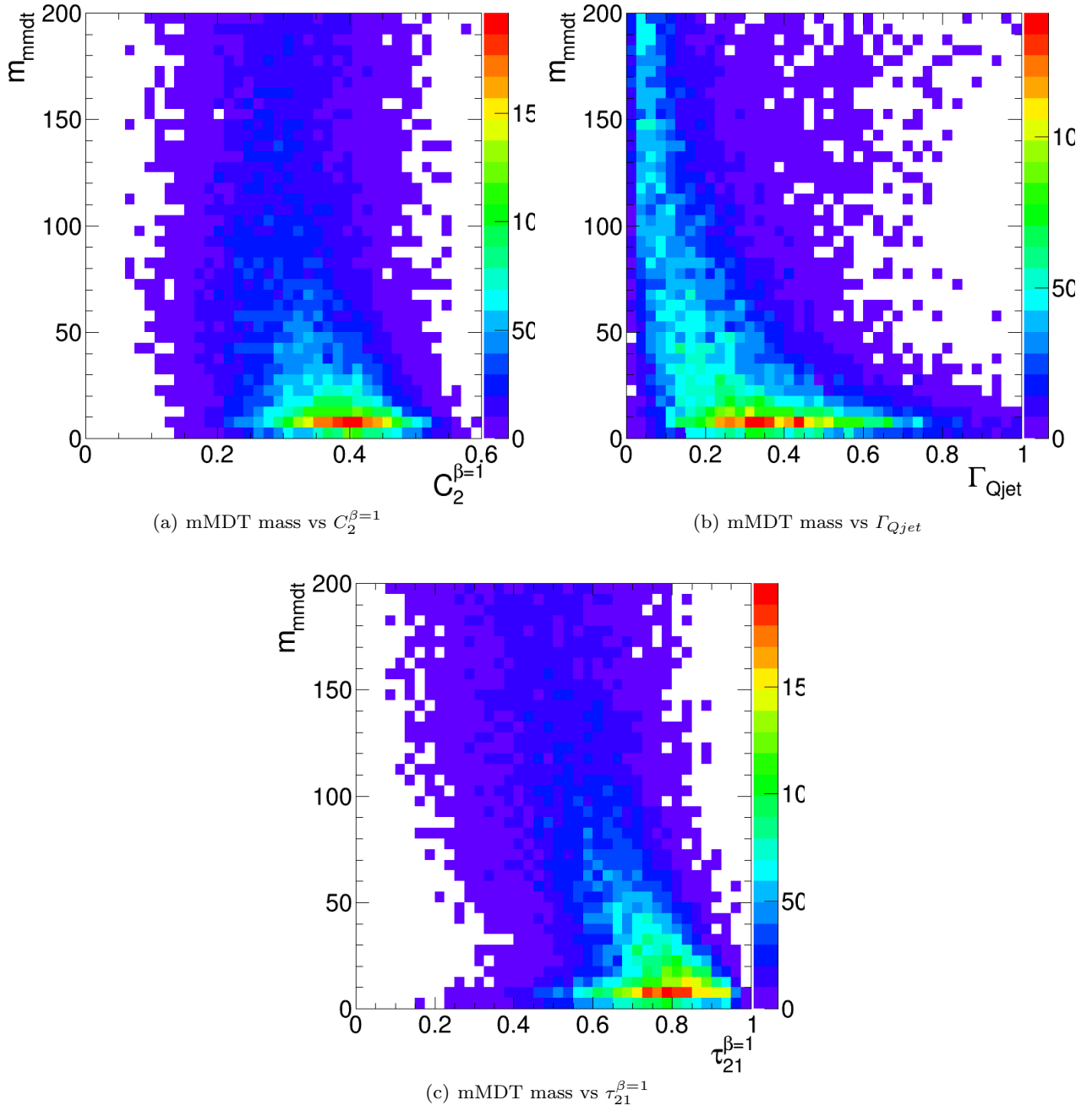(c) mMDT mass vs $\tau_{21}^{\beta=1}$

Fig. 14 2-D plots showing the correlation between mMDT mass and various substructure variables in the p_T 500 GeV bin using the anti-k_T R=1.2 algorithm in the gg sample.
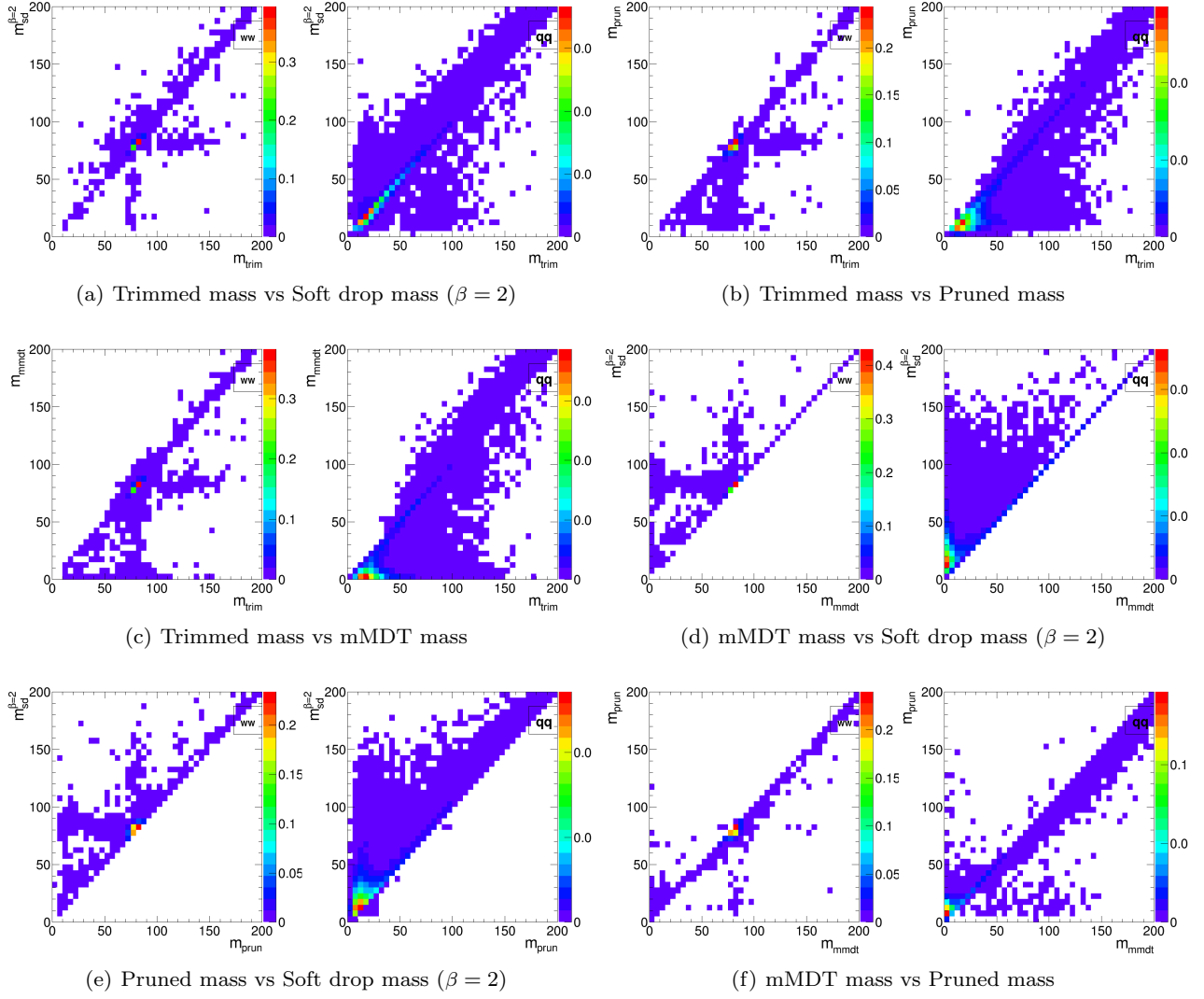
(a) Trimmed mass vs Soft drop mass ($\beta = 2$)

(b) Trimmed mass vs Pruned mass

(c) Trimmed mass vs mMDT mass

(d) mMDT mass vs Soft drop mass ($\beta = 2$)

(e) Pruned mass vs Soft drop mass ($\beta = 2$)

(f) mMDT mass vs Pruned mass

Fig. 15 2-D plots showing the correlation between different types of groomed mass in the p_T 500 GeV bin using the anti-k_T R=0.8 algorithm, separately for the jets in the $X \rightarrow WW$ sample and the jets in the quark-quark sample.
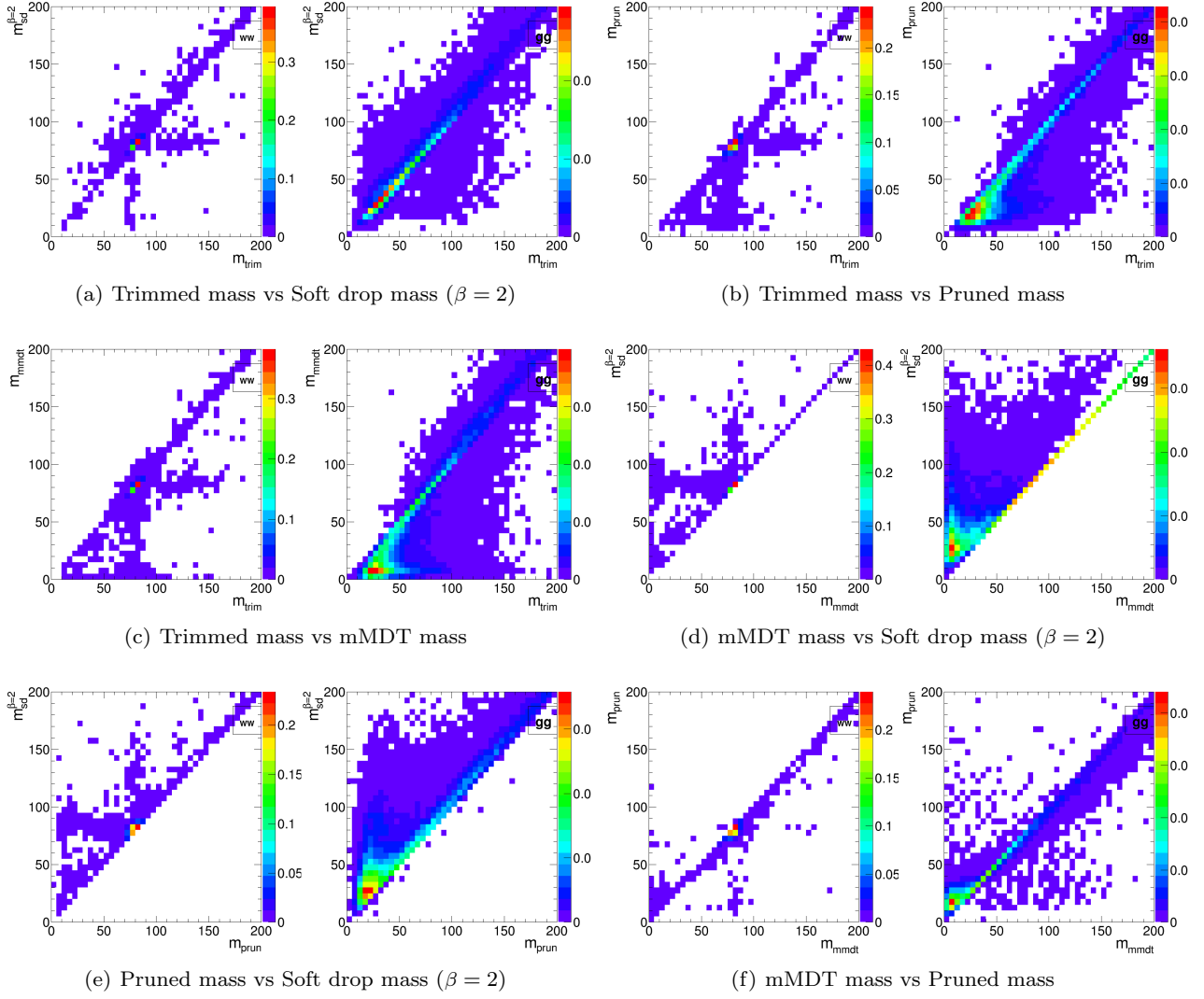
(a) Trimmed mass vs Soft drop mass ($\beta = 2$)

(b) Trimmed mass vs Pruned mass

(c) Trimmed mass vs mMDT mass

(d) mMDT mass vs Soft drop mass ($\beta = 2$)

(e) Pruned mass vs Soft drop mass ($\beta = 2$)

(f) mMDT mass vs Pruned mass

Fig. 16 2-D plots showing the correlation between different types of groomed mass in the p_T 500 GeV bin using the anti-k_T R=0.8 algorithm, separately for the jets in the $X \rightarrow WW$ sample and the jets in the gluon-gluon sample.

7 Top Tagging

In this section, we study the identification of boosted top quarks at Run II of the LHC. Boosted top quarks result in large-radius jets with complex substructure, containing a b-subjet and a boosted W. The additional kinematic handles coming from the reconstruction of the W mass and b-tagging allows a very high degree of discrimination of top quark jets from QCD backgrounds.

We consider top quarks with moderate boost (600-1000 GeV), and perhaps most interestingly, at high boost ($\gtrsim$ 1500 GeV). Top tagging faces several challenges in the high-p_T regime. For such high-p_T jets, the b-tagging efficiencies are no longer reliably known. Also, the top jet can also accompanied by additional radiation with $p_T \sim m_t$, leading to combinatoric ambiguities of reconstructing the top and W, and the possibility that existing taggers or observables shape the background by looking for subjet combinations that reconstruct m_t/m_W. To study this, we examine the performance of both mass-reconstruction variables, as well as shape observables that probe the three-pronged nature of the top jet and the accompanying radiation pattern.

7.1 Methodology

We study a number of top-tagging strategies, in particular:

1. HEPTopTagger
2. Johns Hopkins Tagger (JH)
3. Trimming
4. Pruning

The top taggers have criteria for reconstructing a top and W candidate, while the grooming algorithms (trimming and pruning) do not incorporate a W-identification step. For a level playing field, we construct a W candidate from the three leading subjets by taking the pair of subjets with the smallest invariant mass; in the case that only two subjets are reconstructed, we take the mass of the leading subjet. All of the above taggers and groomers incorporate a step to remove pile-up and other soft radiation.

We also consider the performance of jet shape observables. In particular, we consider the N-subjettiness ratios $\tau_{32}^{\beta=1}$ and $\tau_{21}^{\beta=1}$, energy correlation function ratios $C_3^{\beta=1}$ and $C_2^{\beta=1}$, and the Qjet mass volatility Γ. In addition to the jet shape performance, we combine the jet shapes with the mass-reconstruction methods listed above to determine the optimal combined performance.

To quantify the performance of each tagger, we combine the relevant tagger output observables and jet shapes into a boosted decision tree (BDT), which determines the optimal multivariate cut. Additionally, because each tagger has two inputs (list, or maybe refer back to Section 3), we scan over reasonable values of the inputs to determine the optimal value for each top tagging signal efficiency. This allows a direct comparison of the optimized version of each tagger.

(a) HEPTopTagger

(b) Johns Hopkins Tagger

(c) Pruning

(d) Trimming

(e) HEP+JH comparison

(f) Grooming comparison
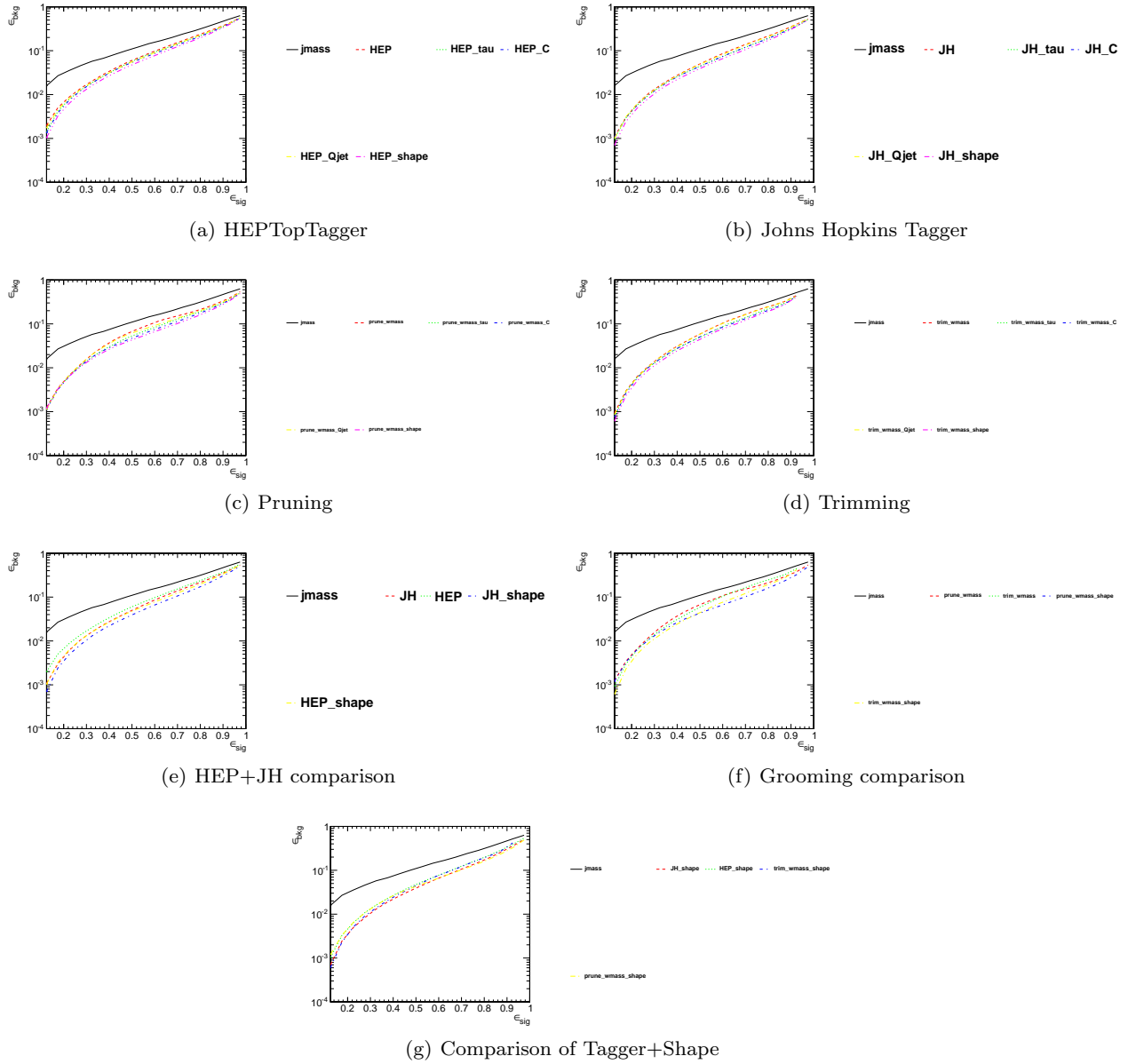
(g) Comparison of Tagger+Shape

Fig. 17 The BDT combinations in the p_T 500 GeV bin using the anti-k_T R=0.8 algorithm.

7.2 Performance at moderate boost

7.3 Performance at high boost

7.4 Direct comparison at different boost

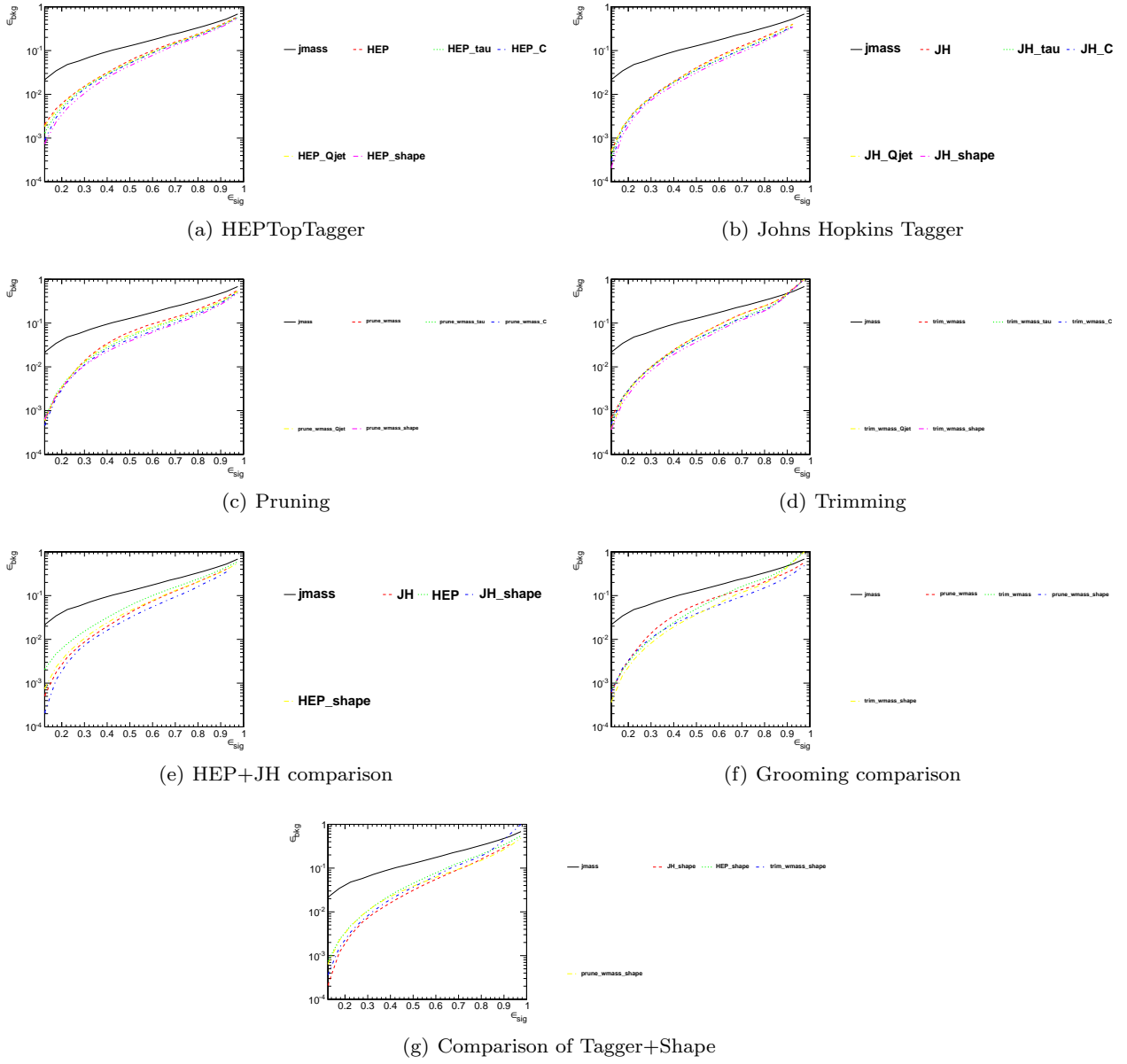## 7.5 Direct comparison at different radius

(a) HEPTopTagger

(b) Johns Hopkins Tagger

(c) Pruning

(d) Trimming

(e) HEP+JH comparison

(f) Grooming comparison

(g) Comparison of Tagger+Shape

Fig. 18 The BDT combinations in the p_T 1000 GeV bin using the anti-k_T R=0.8 algorithm.

(a) HEPTopTagger

(b) Johns Hopkins Tagger

(c) Pruning

(d) Trimming

(e) HEP+JH comparison

(f) Grooming comparison

(g) Comparison of Tagger+Shape

Fig. 19 The BDT combinations in the p_T 1500 GeV bin using the anti-k_{T} R=0.8 algorithm.

(a) C2

(b) C3

(c) τ_{21}

(d) τ_{32}

(e) Mass volatility

(f) HEPTopTagger

(g) Johns Hopkins Tagger

(h) Trimming

(i) Pruning

Fig. 20 Comparison of tagger and jet shape performance at different p_T using the anti-k_T R=0.8 algorithm.

(a) C2

(b) C3

(c) τ_{21}

(d) τ_{32}

(e) Mass volatility

(f) HEPTopTagger

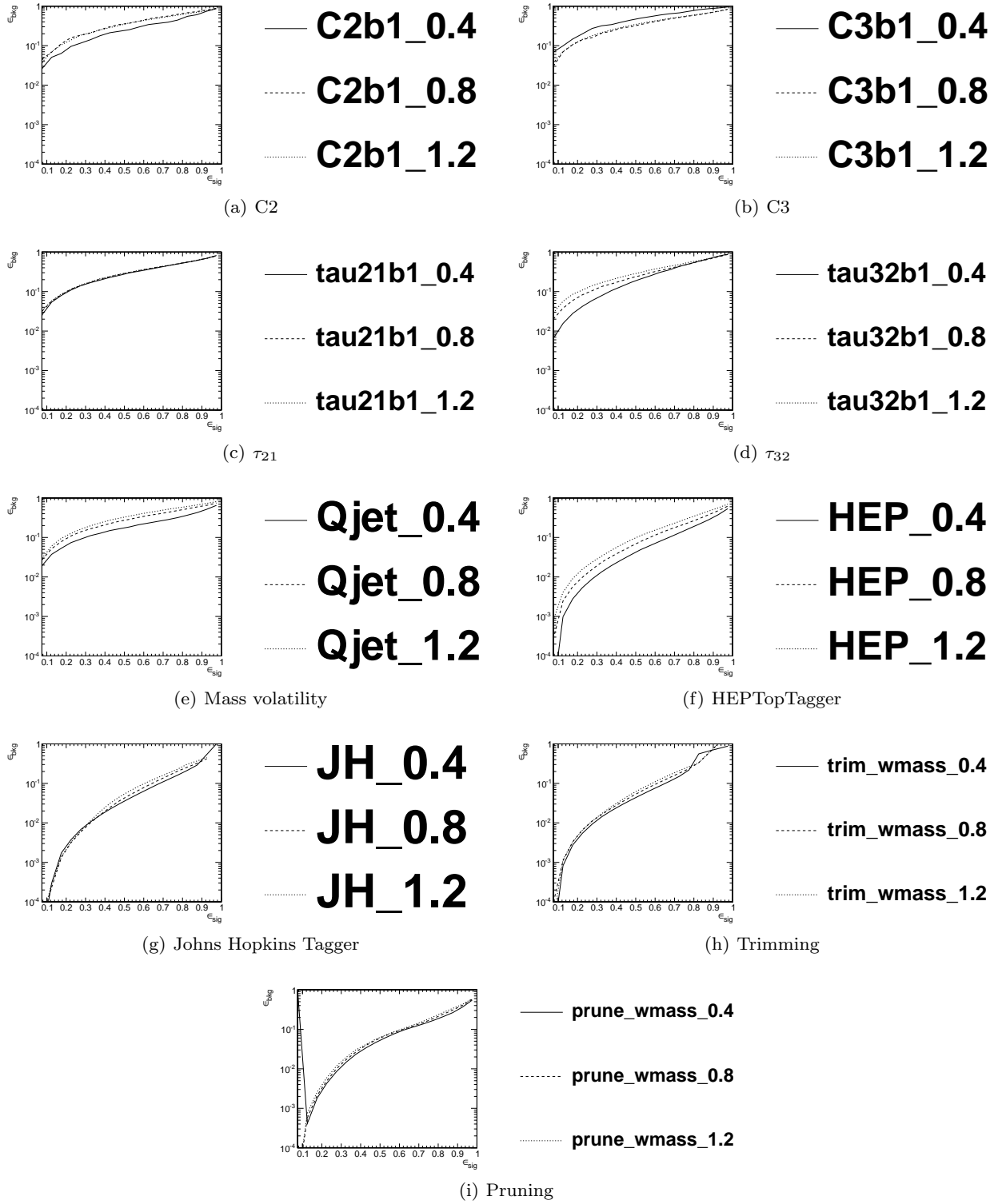(g) Johns Hopkins Tagger

(h) Trimming

(i) Pruning

Fig. 21 Comparison of tagger and jet shape performance at different radius at $p_T = 1.5$ TeV.

8 Summary & Conclusions

This report discussed the correlations between observables and looked forward to jet substructure at Run II of the LHC at 14 TeV center-of-mass collisions eneergies.

Acknowledgements

We thank the Department of Physics at the University of Arizona and for hosting the conference at the Little America Hotel. We also thank Harvard University for

hosting the event samples used in this report. We also thank Hallie Bolonkin for the BOOST2013 poster design and Jackson Boelts' ART465 class (fall 2012) at the University of Arizona School of Arts VisCom program. (NEED TO ASK PETER LOCH FOR MORE ACKNOWLEDGEMENTS)

References

1. A. Abdesselam, E. B. Kuutmann, U. Bitenc, G. Brooijmans, J. Butterworth, et al., *Boosted objects: A Probe of beyond the Standard Model physics*, *Eur.Phys.J.* **C71** (2011) 1661, [`arXiv:1012.5412`].
2. A. Altheimer, S. Arora, L. Asquith, G. Brooijmans, J. Butterworth, et al., *Jet Substructure at the Tevatron and LHC: New results, new tools, new benchmarks*, *J.Phys.* **G39** (2012) 063001, [`arXiv:1201.0008`].
3. A. Altheimer, A. Arce, L. Asquith, J. Backus Mayes, E. Bergeaas Kuutmann, et al., *Boosted objects and jet substructure at the LHC*, `arXiv:1311.2708`.